Journal of Electroanalytical Chemistry 877 (2020) 114485

Contents lists available at ScienceDirect

Journal of Electroanalytical Chemistry

journal homepage: www.elsevier.com/locate/jelechem

Growth and electrochemical stability of a layer-by-layer thin film containing tetrasulfonated Fe phthalocyanine

Federico G. Davia, Nicolas P. Johner [1], Ernesto J. Calvo, Federico J. Williams *

Departamento de Química Inorgánica, Analítica y Química Física, Facultad de Ciencias Exactas y Naturales, INQUIMAE-CONICET, Universidad de Buenos Aires, Ciudad Universitaria, Pabellón II, Buenos Aires C1428EHA, Argentina

ARTICLE INFO

Article history:
Received 3 March 2020
Received in revised form 5 July 2020
Accepted 8 July 2020
Available online 29 July 2020

Keywords:
Fe phthalocyanine
Oxygen reduction reaction
Layer-by-layer
Polyallylamine
Thin films
Electrocatalysis

ABSTRACT

Devices based on the functionalization of surfaces with iron phthalocyanine could have potential applications in sensors as well as in clean energy generation. In this work we studied the growth and electrochemical stability of layer-by-layer (LbL) thin films composed of alternating layers of anionic iron tetrasulfonated phthalocyanine (FeTsPc) and cationic polyallylamine (PAH). Atomic force microscopy (AFM) was used to monitor film morphology and X-ray photoelectron spectroscopy (XPS) was used to monitor the film chemical composition. Films grow uniformly increasing their thickness as the number of deposited layers increases. Cyclic voltammetry (CV) was used to determine the electrochemical activity for the oxygen reduction reaction (ORR). Thin films with 1, 3, 5 and 10 FeTsPc/PAH bilayers show similar activities for the ORR after cycling 50 times. Post-electrochemical AFM and XPS show that the film restructures after electrochemical cycling forming deposits with electrochemical activities close to that of a monolayer of FeTsPc. Our results are important for the design of LbL films incorporating catalytically active redox centers.

1. Introduction

The electrochemical conversion of hydrogen and oxygen into water could be used for clean energy generation employing polymer electrolyte fuel cells [1]. However, in order to advance the technology it is necessary to develop non-platinum group metal catalysts for the oxygen reduction reaction (ORR) [2,3]. Since Co phthalocyanines were first reported to catalyse the ORR [4] a great research effort was undertaken to develop M-N4 catalysts [5], where M-N4 represents a metal atom coordinated by four pyrrolic nitrogen atoms [6,7]. In this group of catalysts, iron phthalocyanines (FePc) have activities comparable to Pt-based catalysts for the ORR in alkaline media favouring the reduction to water (four electron process) instead of hydrogen peroxide (two electron process) [8–10]. Therefore, the reduction of oxygen electrocatalyzed by FePc functionalized electrodes have been studied extensively [11–17].

Polymeric films containing M-N4 macrocycles were designed to improve the stability and the electrocatalytic activity towards oxygen reduction [18–22]. Recently, Tang and co-workers prepared layer-by-layer (LbL) films containing cobalt porphyrins and used them successfully for the reduction of oxygen [23]. In short, LbL films are ultra-thin films of controlled thickness obtained after the sequential deposition of polyelectrolyte layers of alternating charge [24,25]. Electrochemically active redox LbL films can be prepared incorporating different redox molecules [26]. LbL films incorporating FePc centers were obtained after the sequential deposition of anionic tetrasulfonated iron phthalocyanine (FeTsPc) and cationic polyallylamine hydrochloride (PAH) [27]. These systems were shown to be electroactive [28] and were used as sensors for the determination of dopamine [27] and polyphenols [29]. Thus, it is very interesting to determine the electrochemical activity towards oxygen reduction of LbL films containing FeTsPc molecules.

In this work we report the growth of LbL films based on the self-assembly of FeTsPc anions and PAH polycations on highly orientated pyrolized graphite (HOPG) electrodes. Film growth was characterized employing X-ray photoelectron spectroscopy (XPS) and atomic force microscopy (AFM) as a function of deposited layers. Furthermore, the activity for the catalytic reduction of oxygen was determined as a function of film thickness. Our results shed new light into the development of LbL films containing catalytically active centers.

2. Materials and methods

PAH was purchased from Sigma-Aldrich and used without further purification. FeTsPc was synthesized and purified by the procedure described by Weber and Busch [30]. LbL films were assembled onto HOPG substrates.

* Corresponding author.
E-mail address: fwilliams@qi.fcen.uba.ar. (F.J. Williams).
[1] Present address: Department of Chemistry and Pharmacy, Friedrich-Alexander University Erlangen-Nürnberg, Egerlandstraße 3, 91,058 Erlangen, Germany.

http://dx.doi.org/10.1016/j.jelechem.2020.114485

The LbL film deposition was performed using FeTsPc and PAH solutions, both with concentration of 0.5 mg/mL and prepared using a phosphate buffer solution with 0.05 mol/L Na_2HPO_4 and NaH_2PO_4 at pH = 7. The sequential deposition of multilayers was carried out by depositing a drop of the anionic (FeTsPc) solution followed by a drop of the cationic (PAH) solution on the substrate for 5 min. After deposition of each solution drop, the substrate coated with the film was rinsed with MilliQ water. This process was repeated to achieve the desired number of layers.

AFM imaging was performed in air using an Agilent 5500 scanning probe microscope (Agilent Technologies) isolated from vibrations, air turbulence and acoustic noise. Images were acquired using an insulating triangular Si PointProbe Plus Non-Contact/Soft Tapping Mode tip (radius < 10 nm, force constant 48 N m^{-1}, resonance frequency 309.1 kHz) in non-contact mode. Scanning tunneling microscopy imaging was not possible due to unstable tunneling currents. XPS measurements were conducted in an ultrahigh vacuum chamber with a base pressure below 5×10^{-10} mbar, using a 150 mm hemispherical SPECS electron energy analyzer and a Mg Kα X-ray source. The reported binding energies were referenced to the Au $4f_{7/2}$ signal of a Au(111) single crystal at 84 eV. N 1s, S 2p, C 1s and Fe 2p atomic ratios were calculated from the integrated intensities of core levels after instrumental and photoionization cross-section corrections. The electrochemical experiments were performed with an Autolab V 30 (Eco Chemie, Utrecht, The Netherlands). All electrochemical experiments were carried out at room temperature in a purpose-built three electrode Teflon cell. A Pt counter electrode and a Ag/AgCl (3 M KCl) reference electrode were employed. Potentials herein are reported with respect to reversible hydrogen electrode (RHE). Cyclic voltammograms (CV) were performed at 0.1 V/s using a KOH 0.1 M solution (pH = 13) saturated in oxygen leaving an oxygen stream ontop of the solution.

3. Results and discussion

Formation of LbL films containing FeTsPc molecules was carried our by the sequential deposition of FeTsPc and PAH molecules over clean HOPG substrates as illustrated in Fig. 1. After each deposition step the sample was rinsed with water. Layers were deposited using 0.5 mg/mL PAH and FeTsPc solutions (PBS buffer, pH = 7).

Fig. 2 shows AFM images of the bare HOPG substrate and after the deposition of 1, 3, 5 and 10 (FeTsPc/PAH) bilayers. The initial bare HOPG surface (a) shows large terraces separated by monoatomic step edges and confirms the flat nature of the substrate. Bilayer deposition (b)-(e) seems to wet the surface uniformly leaving a few pinholes behind seen as black areas, and some surface aggregates seen as bright dots. The step edges are still distinguished after deposition of the first bilayer indicating its very thin nature but are no longer seen after further bilayer deposition. Furthermore, as the film grows thicker the number of pinholes decreases whereas the size of the surface aggregates seems to increase. Fig. 2 f shows the film thickness as a function of the number of deposited bilayers. Film thickness was estimated using the height of the pinholes that expose the flat HOPG surface. Clearly, as the number of bilayers increases films grow thicker with an estimated thickness of 1.5 nm per bilayer. This is in line with recent profilometry studies that show a linear growth of the film between 10 and 50 bilayers with an average bilayer thickness of 1.1 nm [29]. It should finally be noted that the sharpness of the image corresponding to the thicker film (e) is lower than the previous images, this could be the effect of water uptake as the images were measured in non-contact mode.

Fig. 3 shows the C 1s, N 1s, Fe 2p and S 2p XPS spectra corresponding to the initial HOPG surface and after deposition of 1, 3, 5 and 10 (FeTsPc/PAH) bilayers. The only signal observed in the initial substrate is a C 1s peak centered at 284.5 eV corresponding to HOPG [31]. The complete absence of other signals indicates that the initial surface is chemically clean. The intensity of the HOPG C 1s signal at 284.5 eV decreases as FeTsPc/PAH bilayers are deposited due to the attenuation of the photoelectrons travelling through the film [32]. Furthermore, a new C 1s contribution is observed at higher binding energies due to the C atoms present on both the FeTsPc molecule and the PAH polymer [32–34]. The N 1s XPS signal is composed of two main contributions at 399 eV due to the N atoms in the FeTsPc molecule and amine groups in PAH and at 401.8 eV due to the protonated amine groups in PAH [35]. The Fe 2p XPS signal shows the expected doublet at 709.4 eV (Fe $2p_{3/2}$) and 722.3 eV (Fe $2p_{1/2}$) due to the Fe atoms in the FeTsPc molecule [36]. Finally, the S 2p signal shows an unresolved doublet with the S $2p_{3/2}$ signal at 168.2 eV due to the sulfonate groups in the FeTsPc molecules [37]. The number and position of the different signals observed in XPS are in line with the expected chemical composition of the LbL film.

Fig. 4 shows the N 1s, S 2p and Fe 2p integrated intensities corrected by the corresponding sensitivity factors and normalized with respect to the Fe 2p intensity as a function of the AFM estimated layer thickness. Clearly the signals increase with thickness reaching a saturation value once the thickness of the film is larger than the thickness probed by XPS. If we assume uniform film growth, then the intensity of each signal in the film (I) should grow according to the following expression: $I = I_0\,(1\text{-}e^{d/(\lambda\cos\theta)})$ where d is the film thickness, λ is the photoelectron attenuation length, θ is the emission angle and I_0 is the XPS area of a sufficiently thick film so that the

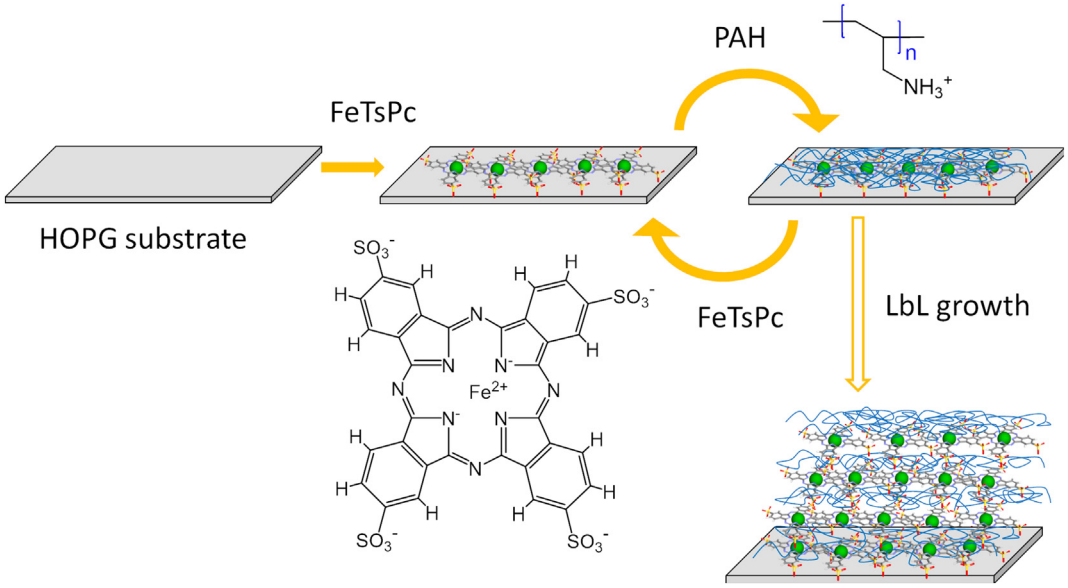

Fig. 1. Schematic illustrating the sequential deposition of FeTsPc and PAH layers on HOPG. Also shown are the molecular structures for both electrolytes.

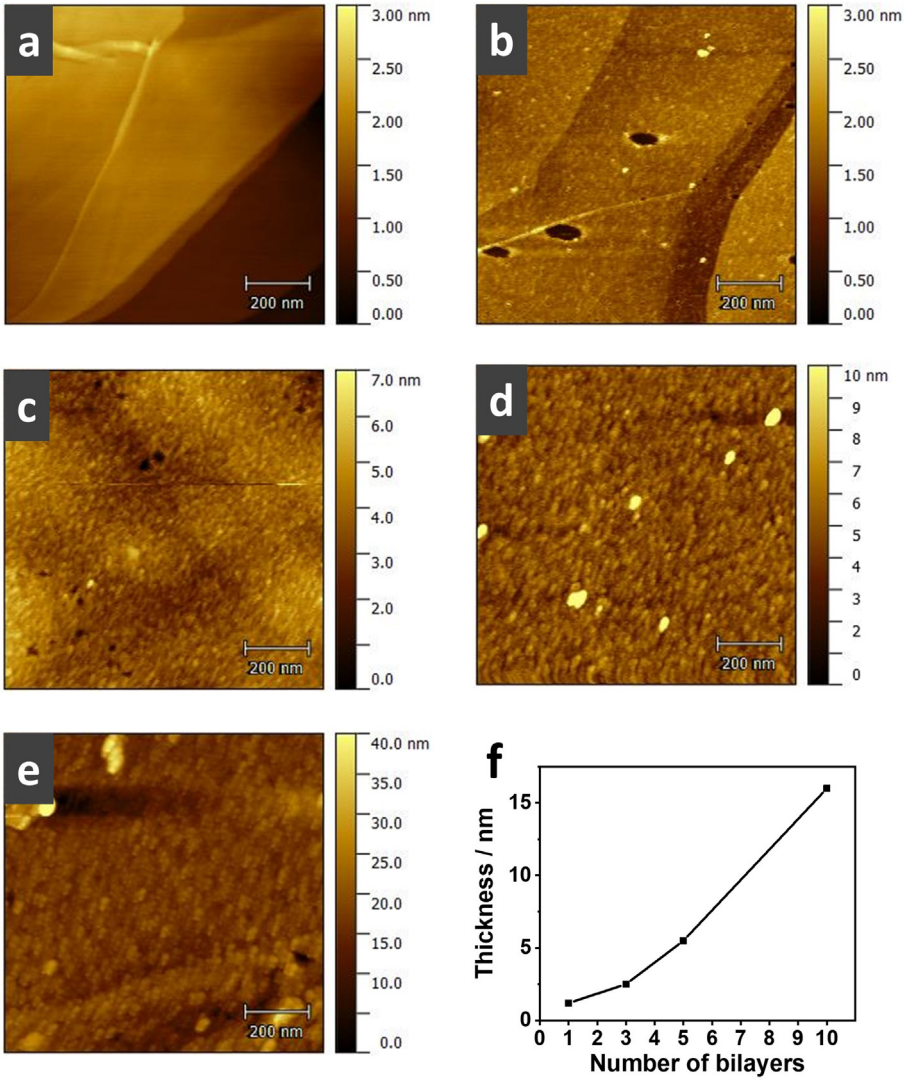

Fig. 2. AFM images of (a) the bare substrate and (b)-(e) after depositing a 1,3,5 and 10 FeTsPc/PAH bilayers. Layers were deposited using 0.5 mg/mL PAH and FeTsPc solutions (PBS buffer, pH = 7). Image (f) shows the film thickness as a function of the number of deposited bilayers.

substrate signal has completely vanished [38]. The data shown in Fig. 3 could be adequately fitted with the above expression as shown by the full lines. This suggests that film growth is uniform. Furthermore, from the XPS integrated areas we can calculate the elemental ratios. Indeed, the corrected XPS Fe:S ratio is close to 1: 4 in agreement with the stoichiometry of the FeTsPc molecule and the Fe:N ratio is close to 1:20 indicating 12 monomers per phthalocyanine molecule in the film.

The stratified nature of the LbL film composed of alternating layers of FeTsPc and PAH could be demonstrated with XPS. A closer look at the data in Fig. 4 reveals that when the film terminates in an FeTsPc layer (open circles) the N 1s intensity (mainly due to PAH) decreases slightly and the Fe 2p and S 2p signals increase slightly. On the contrary, when a film terminates in a PAH layer (closed circles) the Fe 2p and S 2p intensities due to FeTsPc decrease slightly whereas the N 1s signal (mainly due to PAH) increases slightly. This indicates that each deposited layer grows ontop of an oppositely charged layer attenuating the XPS signals of elements from the buried layer. This is in complete agreement with vibrational studies of the same LbL film grown under the same conditions showing that the interaction between sulfonate groups and protonated amine groups bind the alternate layers [27]. However, this is not the only interaction between layers as the Fe centers in FeTsPc molecules coordinate $-NH_2$ groups from neighbouring PAH molecules [27].

It is instructive to follow the intensity of the sodium counterions balancing charges on the film. Fig. 5 (a) shows Na 1s XPS spectra as a function of the number of deposited bilayers, where fractional bilayers numbers indicate FeTsPc terminated films, ie. a bilayer number of 0.5 indicates a film composed of a single layer of FeTsPc molecules. The Na 1s XPS spectrum corresponding to the FeTsPc monolayer shows the presence of Na^+ present as counterions of the anionic sulfonate groups in FeTsPc molecules. When a PAH layer is deposited ontop, there is charge overcompensation [39] and the ammonium ions in the polymer interact with sulfonate groups releasing sodium cations into the solution, thus the sodium XPS signal decreases in PAH terminated films. A further deposition of a FeTsPc layer overcompensates charges again and thus the Na 1s XPS signal in FeTsPc terminated films increases. This is exactly what we observe in Fig. 5 (b) indicating that FeTsPc/PAH films grow in a layer by layer fashion via the electrostatic interaction of oppositely charged ions present in each alternating layer as expected.

The AFM and XPS data discussed above confirm that the sequential deposition of FeTsPc and PAH results in uniform thin films of growing thickness that incorporate the catalytically active redox center in growing numbers. In order to test if the redox centers in the LbL films are catalytically active towards the ORR cyclic voltammograms (CV) in the presence of oxygen were carried out. Fig. 6 (a) shows three consecutive CVs measured using the HOPG electrode functionalized with a 5 bilayer film at

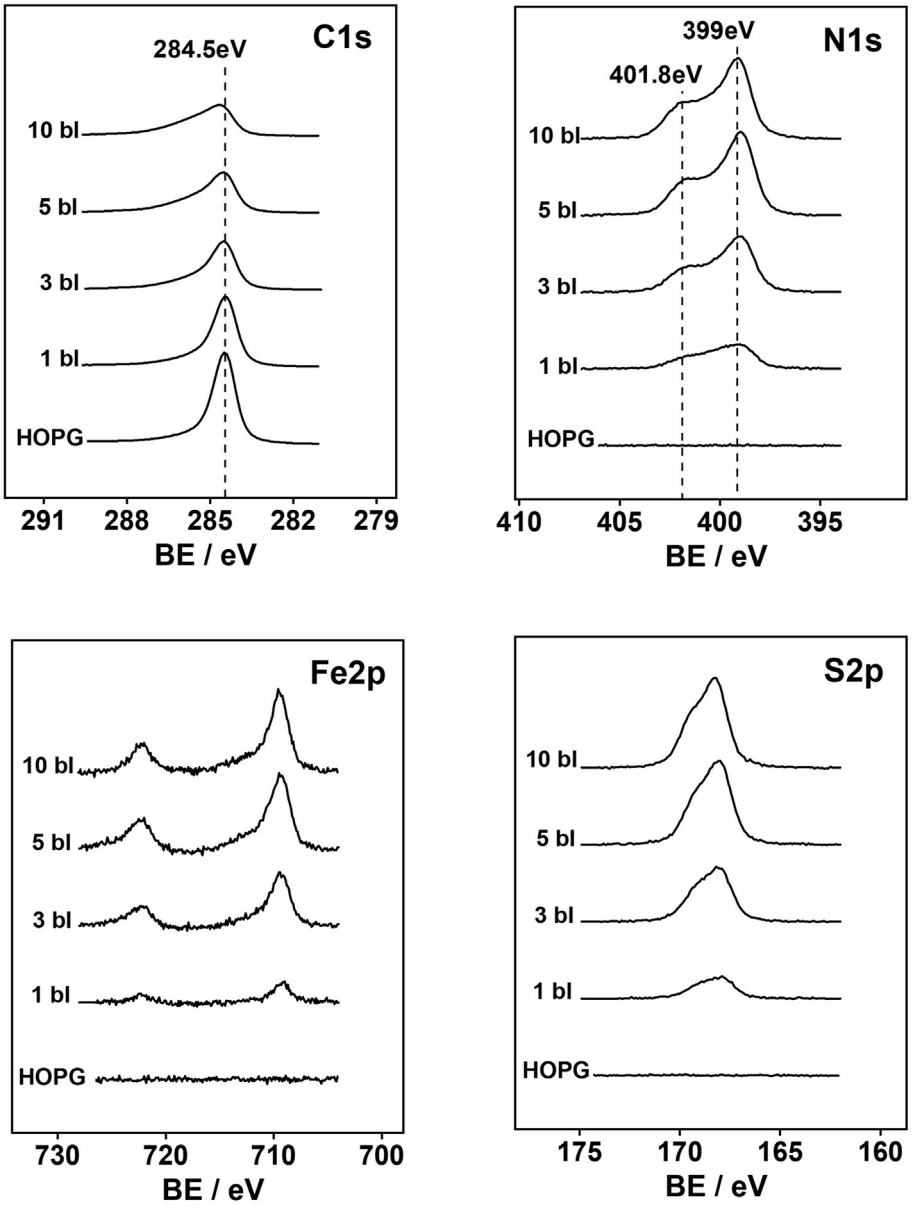

Fig. 3. XPS spectra corresponding to the bare HOPG substrate and after depositing LbL films with a different number of FeTsPc/PAH bilayers. Layers were deposited using 0.5 mg/mL PAH and FeTsPc solutions (PBS buffer, pH = 7).

pH = 13. As the electrochemical potential is decreased below 0.9 V versus the reversible hydrogen electrode (RHE) all curves show a cathodic wave due to the reduction of oxygen to water [8]. Furthermore, as the number of cycles increases the electrochemical activity of the film increases to reach a reproducible behaviour maintained beyond 50 cycles. The same behaviour was observed using thin films terminated with FeTsPc molecules and with a different number of bilayers. As mentioned above initially the Fe centers could be coordinating $–NH_2$ groups and therefore could be blocked from interacting with O_2 molecules, hence in the first CV the charge is relatively small. Once the O_2 molecules bind to more Fe centers the charge increases. This breaks the bonding between Fe and the $–NH_2$ groups weakening the interactions between layers. As we should see below electrochemical cycling has a large impact on the stratified structure of the film.

Fig. 6 (b) shows a CV measured after carrying out 50 cycles using electrodes functionalized with thin films of growing bilayer number. Clearly, the same overall behaviour is observed in all cases, i.e. the onset potential as well as the electrochemical activity are quite similar independently of the number of deposited layers. Also, all curves show two overlapping peaks which are the characteristic oxygen reduction peaks observed in graphite electrodes modified with FeTsPc molecules [8]. Fig. 6 (c) shows CVs measured in the presence and absence of O_2 for LbL films terminated with either FeTsPC (4.5 bilayers) or PAH (5 bilayers) molecules. Clearly, the observed curves are due to the reduction of O_2 and the same behaviour is observed for LbL films terminated with either FeTsPc or PAH. This is due to the changes that take place in the film structure during electrochemical operation as discussed below.

The measurements discussed above show that the electrochemical behaviour is independent of layer number and termination. In order to rationalize this post-ORR ex situ AFM and XPS measurements were carried out. Fig. 7 shows AFM images of a 10 bilayer thin film measured (a) before and (b) after performing 50 electrochemical cycles when the catalytic activity remains constant. As shown in Fig. 7 (a), initially the thin film covers the surface uniformly with an average thickness of around 15 nm and leaving behind some small holes and some agglomerates. This morphology changes drastically after performing 50 electrochemical cycles reducing oxygen

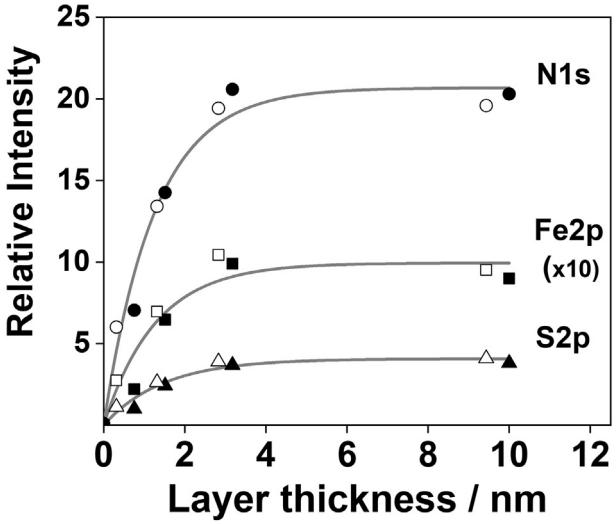

Fig. 4. N 1 s, S 2p and Fe 2p XPS integrated intensities normalized with respect to the Fe 2p intensity as a function of layer thickness. Open circles correspond to FeTsPc terminated layers whereas close circles correspond to PAH terminated layers.

(Fig. 7 (b)). In this case steps separating terraces have become clearly visible and the film does not seem to be covering the surface uniformly, instead the film restructures with a drastic film thickness reduction.

Fig. 8 shows the C 1s, N 1s, Fe 2p and S 2p XPS spectra of a 10 bilayer thin film measured before (black curves) and after (red curves) carrying out 50 electrochemical cycles reducing oxygen. The C 1s signal shows a significant increase in the 284.5 eV substrate signal and a decrease in the higher binding energy shoulder due to the LbL film. This indicates a reduction of film thickness and is in line with the AFM results discussed above. The average film thickness could be estimated from the substrate XPS signal resulting in 2 nm in line with the height profiles observed in the post-electrochemical cycling AFM image. This implies an 86% decrease in film thickness after electrochemical cycling. The N 1s, Fe 2p and S 2p XPS signals show a large decrease in intensity after electrochemical cycling. This suggests that many PAH and FeTsPc molecules are lost from the electrode surface resulting in the observed decrease in film thickness. Thus, the fact that ORR is independent of the number of bilayers in the film is explained in terms of the observed film thickness reduction. Note that the corrected Fe:S XPS ratio after cycling remained close to 1:4 indicating that the FeTsPc molecules are not decomposed. The AFM and XPS observed film thickness reduction is in line with the proposed O_2 induced weakening of interlayer interactions discussed above. Here we note that this effect could depend on the pH of the solutions employed to prepare the LbL film.

The data discussed above shows that the sequential deposition of anionic FeTsPc molecules and cationic PAH molecules generate thin films of

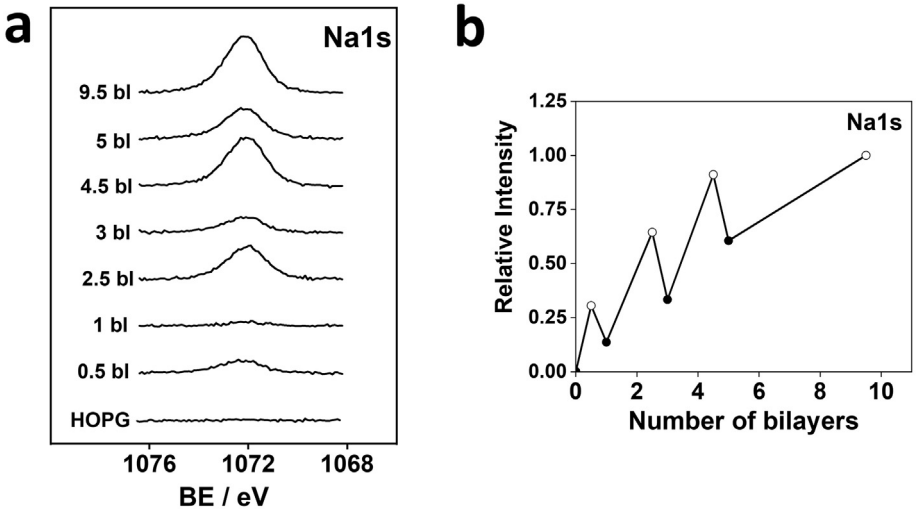

Fig. 5. (a) Na 1 s XPS spectra and (b) integrated intensities as a function of the number of (FeTsPc/PAH) bilayers. Fractional bilayer numbers indicate FeTsPc terminated LbL films (open circles). Integer bilayer numbers indicate PAH terminated films (closed circles).

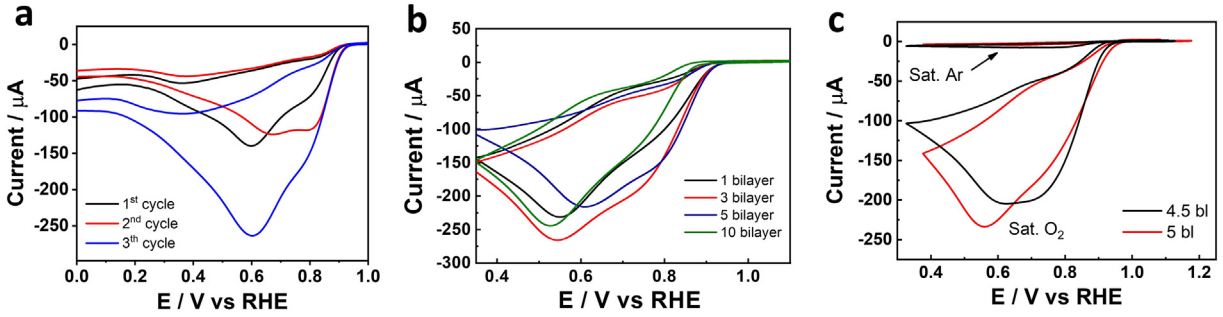

Fig. 6. (a) Consecutive CVs measured using a 5 bilayer thin film in O_2. (b) CVs of electrodes modified with 1, 3, 5 and 10 bilayers measured after 50 cycles in O_2. (c) CVs of electrodes modified with 4.5 (FeTsPc terminated) and 5 (PAH terminated) bilayers measured after 50 cycles in Ar and in O_2. Measurements were performed in KOH 0.1 M after saturating at 0.1 V/s.

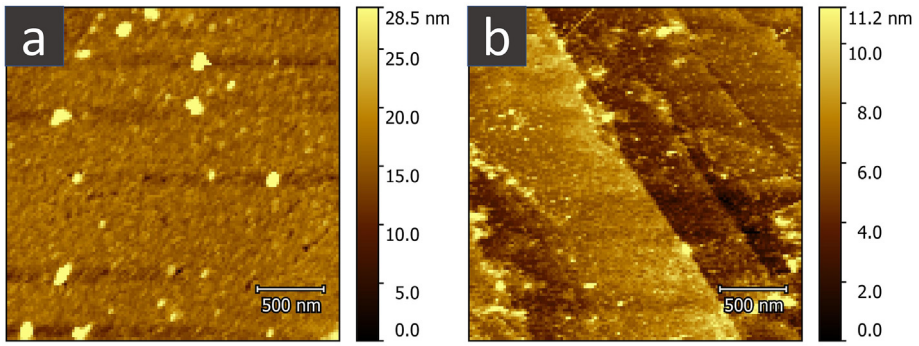

Fig. 7. AFM images of a 10 bilayer film (a) before and (b) after performing 50 electrochemical cycles reducing oxygen in KOH 0.1 M.

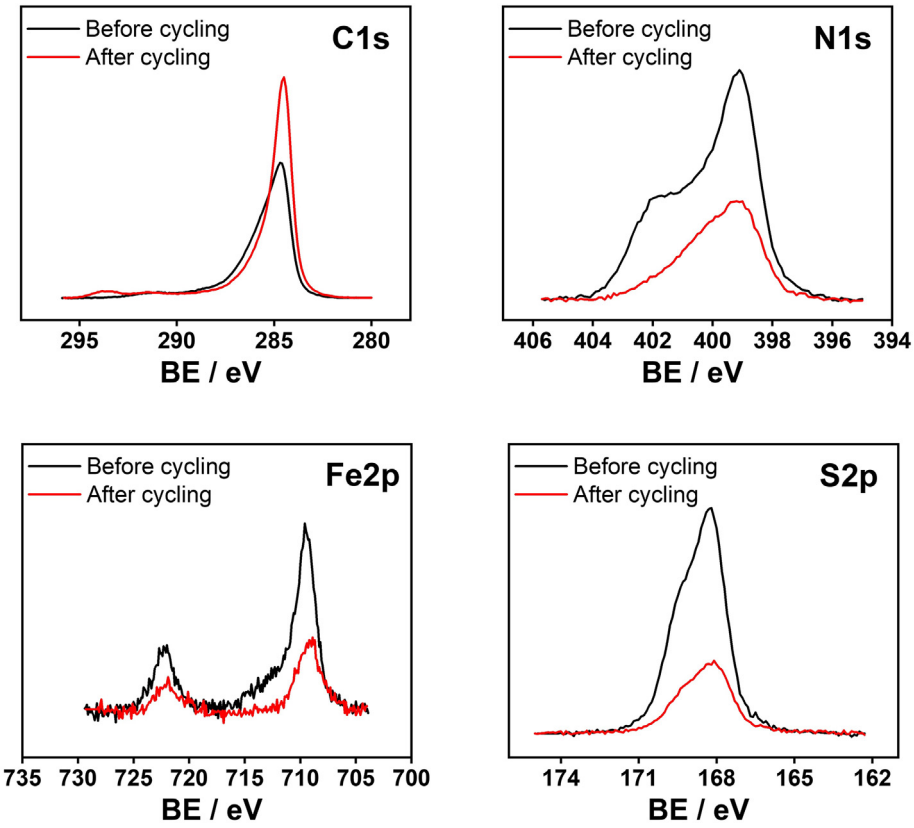

Fig. 8. C 1 s, N 1 s, Fe 2p and S 2p XPS spectra of a 10 bilayer film before (black) and after (red) carrying out 50 electrochemical cycles reducing oxygen in KOH 0.1 M.

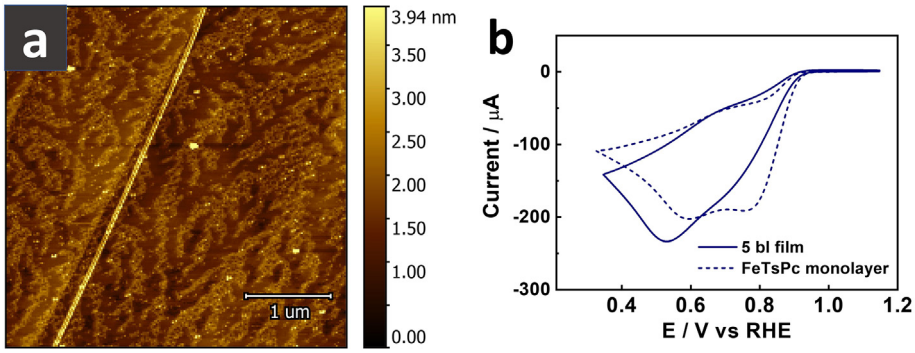

Fig. 9. (a) AFM image of a monolayer of FeTsPc molecules on HOPG after 50 electrochemical cycles in KOH 0.1 M. (b) CVs measured after cycling 5 bilayer film (full lines) and a monolayer film composed of FetSPc (dashed lines) 50 times in an O_2 saturated KOH 0.1 M solution.

controlled thickness and composition. Here we should note that the same films were used successfully as chemical sensors [27,29]. However, we show that after the electrochemical reduction of oxygen films suffer restructuring with a great reduction in thickness. Thus our finding is important as it provides an example of LbL film restructuring under reaction conditions. Finally, we can compare the electrochemical activity of the resulting film to that of a FeTsPc monolayer on HOPG. Fig. 9 (a) shows the AFM image measured after depositing a monolayer of FeTsPc molecules directly onto the HOPG substrate and performing 50 electrochemical cycles reducing oxygen. The molecules in the monolayer form branching structures over the substrate with no aggregation or stacking. Although the nature of the observed structures is at present not understood, their height is 0.4 nm in line with the molecular height, indicating that the surface is composed of flat-lying FeTsPc molecules. Fig. 9 (b) shows CVs of a 5 bilayer film (full line) and a monolayer film (dashed line) measured after cycling 50 times. Clearly, both the potential onset for the reduction of oxygen as well as the electrochemical activity of the resulting LbL film are close to that of the monolayer.

4. Conclusions

Layer-by-layer thin films composed of anionic FeTsPc and cationic PAH molecules can be successfully grown over HOPG substrates. Sequential deposition leads to thicker films with smaller pinholes and larger corrugation. The number of FeTsPc molecules incorporated into the film increases sharply as the film grows thicker. However, this is not reflected in the electrochemical activity towards ORR. Films with 1, 3, 5 and 10 bilayers, ie. with a growing number of the catalytically active centers, show similar activities towards ORR after 50 electrochemical cycles. Post-electrochemical reaction AFM and XPS measurements show that after extensive electrochemical cycling the polyelectrolyte film restructures suffering a great decreased in film thickness leaving behind 2 nm deposits containing FeTsPc molecules and exposing the bare surface. These deposits are still active for the ORR with electrochemical activities approaching that of an FeTsPc monolayer. The decreased in film thickness can be explained by an O_2 induced weakening of the interlayer interaction by breaking the bonding between $–NH_2$ groups and Fe centers. These findings show that LbL films containing molecular catalysts could lose their stratified nature under reaction condictions and thus they are relevant for the design of LbL films containing catalytically active redox centers.

Declaration of Competing Interest

The authors declare that they have no known competing financial interests or personal relationships that could have appeared to influence the work reported in this paper.

Acknowledgements

The authors acknowledge support from the Consejo Nacional de Investigaciones Científicas y Técnicas (CONICET). F. G. D. thanks YPF Tecnología for a fellowship.

References

[1] M.K. Debe, Electrocatalyst approaches and challenges for automotive fuel cells, Nature 486 (7401) (2012) 43–51, https://doi.org/10.1038/nature11115.
[2] D.J. Berger, Fuel cells and precious-metal catalysts, Science 286 (5437) (1999) 49, https://doi.org/10.1126/science.286.5437.49c.
[3] Z. Chen, D. Higgins, A. Yu, L. Zhang, J. Zhang, A review on non-precious metal electrocatalysts for PEM fuel cells, Energy Environ. Sci. 4 (9) (2011) 3167, https://doi.org/10.1039/c0ee00558d.
[4] R. Jasinski, A new fuel cell cathode catalyst, Nature 201 (4925) (1964) 1212–1213, https://doi.org/10.1038/2011212a0.
[5] J.H. Zagal, F. Bedioui (Eds.), Electrochemistry of N4 Macrocyclic Metal Complexes, Springer International Publishing, Cham, 2016https://doi.org/10.1007/978-3-319-31172-2.
[6] L. Dai, Y. Xue, L. Qu, H.-J. Choi, J.-B. Baek, Metal-free catalysts for oxygen reduction reaction, Chem. Rev. 115 (11) (2015) 4823–4892, https://doi.org/10.1021/cr5003563.
[7] Y. Nie, L. Li, Z. Wei, Recent advancements in Pt and Pt-free catalysts for oxygen reduction reaction, Chem. Soc. Rev. 44 (8) (2015) 2168–2201, https://doi.org/10.1039/C4CS00484A.
[8] J. Zagal, P. Bindra, E. Yeager, A mechanistic study of O_2 reduction on water soluble phthalocyanines adsorbed on graphite electrodes, J. Electrochem. Soc. 127 (7) (1980) 1506, https://doi.org/10.1149/1.2129940.
[9] J. Zagal, M. Páez, A. Tanaka, J. dos Santos, C. Linkous, Electrocatalytic activity of metal phthalocyanines for oxygen reduction, J. Electroanal. Chem. 339 (1–2) (1992) 13–30, https://doi.org/10.1016/0022-0728(92)80442-7.
[10] G. Abarca, M. Viera, C. Aliaga, J.F. Marco, W. Orellana, J.H. Zagal, F. Tasca, In search of the most active MN4 catalyst for the oxygen reduction reaction. The case of perfluorinated Fe phthalocyanine, J. Mater. Chem. A 7 (43) (2019) 24776–24783, https://doi.org/10.1039/C9TA09125D.
[11] X. Hu, D. Xia, L. Zhang, J. Zhang, High crystallinity binuclear iron phthalocyanine catalyst with enhanced performance for oxygen reduction reaction, J. Power Sources 231 (2013) 91–96, https://doi.org/10.1016/j.jpowsour.2012.12.018.
[12] Y. Liu, Y.-Y. Wu, G.-J. Lv, T. Pu, X.-Q. He, L.-L. Cui, Iron(II) phthalocyanine covalently functionalized graphene as a highly efficient non-precious-metal catalyst for the oxygen reduction reaction in alkaline media, Electrochim. Acta 112 (2013) 269–278, https://doi.org/10.1016/j.electacta.2013.08.174.
[13] J. Chlistunoff, J.-M. Sansiñena, Effects of axial coordination of the metal center on the activity of iron tetraphenylporphyrin as a nonprecious catalyst for oxygen reduction, J. Phys. Chem. C 118 (33) (2014) 19139–19149, https://doi.org/10.1021/jp5044249.
[14] R. Chen, H. Li, D. Chu, G. Wang, Unraveling oxygen reduction reaction mechanisms on carbon-supported Fe-phthalocyanine and Co-phthalocyanine catalysts in alkaline solutions, J. Phys. Chem. C 113 (48) (2009) 20689–20697, https://doi.org/10.1021/jp906408y.
[15] Y. Jiang, Y. Lu, X. Lv, D. Han, Q. Zhang, L. Niu, W. Chen, Enhanced catalytic performance of Pt-free iron phthalocyanine by graphene support for efficient oxygen reduction reaction, ACS Catal. 3 (6) (2013) 1263–1271, https://doi.org/10.1021/cs4001927.
[16] J. Govan, W. Orellana, J.H. Zagal, F. Tasca, Penta-coordinated transition metal macrocycles as electrocatalysts for the oxygen reduction reaction, J. Solid State Electrochem. (2020) https://doi.org/10.1007/s10008-019-04489-x.
[17] N. Zion, A. Friedman, N. Levy, L. Elbaz, Bioinspired electrocatalysis of oxygen reduction reaction in fuel cells using molecular catalysts, Adv. Mater. 30 (41) (2018) 1800406, https://doi.org/10.1002/adma.201800406.
[18] C. Coutanceau, P. Crouigneau, J. Léger, C. Lamy, Mechanism of oxygen electroreduction at polypyrrole electrodes modified by cobalt phthalocyanine, J. Electroanal. Chem. 379 (1–2) (1994) 389–397, https://doi.org/10.1016/0022-0728(94)87162-0.
[19] C. Coutanceau, A. El Hourch, P. Crouigneau, J. Leger, C. Lamy, Conducting polymer electrodes modified by metal tetrasulfonated phthalocyanines: preparation and electrocatalytic behaviour towards dioxygen reduction in acid medium, Electrochim. Acta 40 (17) (1995) 2739–2748, https://doi.org/10.1016/0013-4686(95)00263-E.
[20] A. Okunola, B. Kowalewska, M. Bron, P.J. Kulesza, W. Schuhmann, Electrocatalytic reduction of oxygen at electropolymerized films of metalloporphyrins deposited onto multi-walled carbon nanotubes, Electrochim. Acta 54 (7) (2009) 1954–1960, https://doi.org/10.1016/j.electacta.2008.07.077.
[21] S. Zoladek, I.A. Rutkowska, M. Blicharska, K. Skorupska, P.J. Kulesza, Enhancement of oxygen reduction at Co-porphyrin catalyst by supporting onto hybrid multilayered film of polypyrrole and polyoxometalate-modified gold nanoparticles, J. Solid State Electrochem. 20 (4) (2016) 1199–1208, https://doi.org/10.1007/s10008-016-3135-5.
[22] T. Sawaguchi, T. Matsue, K. Itaya, I. Uchida, Electrochemical catalytic reduction of molecular oxygen by iron porphyrin ion-complex modified electrode, Electrochim. Acta 36 (3–4) (1991) 703–708, https://doi.org/10.1016/0013-4686(91)85161-Y.
[23] H. Tang, H. Yin, J. Wang, N. Yang, D. Wang, Z. Tang, Molecular architecture of cobalt porphyrin multilayers on reduced graphene oxide sheets for high-performance oxygen reduction reaction, Angew. Chem. Int. Ed. 52 (21) (2013) 5585–5589, https://doi.org/10.1002/anie.201300711.
[24] G. Decher, Fuzzy nanoassemblies: toward layered polymeric multicomposites, Science 277 (5330) (1997) 1232–1237, https://doi.org/10.1126/science.277.5330.1232.
[25] G. Decher, J.B. Schlenoff (Eds.), Multilayer Thin Films, Wiley-VCH Verlag GmbH & Co. KGaA, Weinheim, Germany, 2012 https://doi.org/10.1002/9783527646746.
[26] E.J. Calvo, Electrochemically active LbL multilayer films: From biosensors to nanocatalysts, Multilayer Thin Films, Wiley-VCH Verlag GmbH & Co. KGaA, Weinheim, Germany 2012, pp. 1003–1038, https://doi.org/10.1002/9783527646746.ch42.
[27] V. Zucolotto, M. Ferreira, M.R. Cordeiro, C.J.L. Constantino, D.T. Balogh, A.R. Zanatta, W.C. Moreira, O.N. Oliveira, Unusual interactions binding iron tetrasulfonated phthalocyanine and poly(allylamine hydrochloride) in layer-by-layer films, J. Phys. Chem. B 107 (16) (2003) 3733–3737, https://doi.org/10.1021/jp027573d.
[28] V. Zucolotto, M. Ferreira, M. Cordeiro, C. Constantino, W. Moreira, O. Oliveira, Electroactive layer-by-layer films of iron tetrasulfonated phthalocyanine, Synth. Met. 137 (1–3) (2003) 945–946, https://doi.org/10.1016/S0379-6779(02)00942-6.
[29] M.D. Maximino, C.S. Martin, F.V. Paulovich, P. Alessio, Layer-by-layer thin film of iron phthalocyanine as a simple and fast sensor for polyphenol determination in tea samples, J. Food Sci. 81 (10) (2016) C2344–C2351, https://doi.org/10.1111/1750-3841.13394.
[30] J.H. Weber, D.H. Busch, Complexes derived from strong field ligands. XIX. Magnetic properties of transition metal derivatives of 4,4′,4″,4‴-tetrasulfophthalocyanine, Inorg. Chem. 4 (4) (1965) 469–471, https://doi.org/10.1021/ic50026a007.
[31] F. Marchini, S.E. Herrera, E.J. Calvo, F.J. Williams, Surface studies of lithium–oxygen redox reactions over HOPG, Surf. Sci. 646 (2016) 154–159, https://doi.org/10.1016/j.susc.2015.07.028.
[32] P. Scodeller, F.J. Williams, E.J. Calvo, XPS analysis of enzyme and mediator at the surface of a layer-by-layer self-assembled wired enzyme electrode, Anal. Chem. 86 (24) (2014) 12180–12184, https://doi.org/10.1021/ac503147c.

[33] C. Isvoranu, J. Åhlund, B. Wang, E. Ataman, N. Mårtensson, C. Puglia, J.N. Andersen, M.-L. Bocquet, J. Schnadt, Electron spectroscopy study of the initial stages of iron phthalocyanine growth on highly oriented pyrolitic graphite, J. Chem. Phys. 131 (21) (2009) 214709, https://doi.org/10.1063/1.3259699.
[34] E. Völker, E.J. Calvo, F.J. Williams, Layer-by-layer self-assembled redox polyelectrolytes on passive steel, Israel J. Chem. 48 (3–4) (2008) 305–312, https://doi.org/10.1560/IJC.48.3-4.305.
[35] M. Tagliazucchi, F.J. Williams, E.J. Calvo, Effect of acid base equilibria on the donnan potential of layer by layer redox polyelectrolyte multilayers, J. Phys. Chem. B 111 (28) (2007) 8105–8113, https://doi.org/10.1021/jp071867n.
[36] C. Isvoranu, B. Wang, E. Ataman, J. Knudsen, K. Schulte, J.N. Andersen, M.-L. Bocquet, J. Schnadt, Comparison of the carbonyl and nitrosyl complexes formed by adsorption of CO and NO on monolayers of iron phthalocyanine on Au(111), J. Phys. Chem. C 115 (50) (2011) 24718–24727, https://doi.org/10.1021/jp204461k.
[37] P. Zhao, L. Niu, L. Huang, F. Zhang, Electrochemical and XPS investigation of phthalocyanine oligomer sulfonate as a corrosion inhibitor for Iron in hydrochloric acid, J. Electrochem. Soc. 155 (10) (2008) C515, https://doi.org/10.1149/1.2967187.
[38] S. Hofmann, Auger- and X-Ray Photoelectron Spectroscopy in Materials Science, Vol. 49 of Springer Series in Surface Sciences, Springer Berlin Heidelberg, Berlin, Heidelberg, 2013 https://doi.org/10.1007/978-3-642-27381-0.
[39] J.B. Schlenoff, S.T. Dubas, Mechanism of polyelectrolyte multilayer growth: charge overcompensation and distribution, Macromolecules 34 (3) (2001) 592–598, https://doi.org/10.1021/ma0003093.